DTU Library

Effects of Different Fuel Specifications and Operation Conditions on the Performance of Coated and Uncoated Superheater Tubes in Two Different Biomass-Fired Boilers

Wu, Duoli; Dahl, Kristian Vinter; Madsen, Jesper L.; Christiansen, Thomas Lundin; Montgomery, Melanie; Hald, John

Effects of Different Fuel Specifications and Operation Conditions on the Performance of Coated and Uncoated Superheater Tubes in Two Different Biomass Fired Boilers

Duoli Wu [a,b] [*], Kristian V. Dahl [b], Jesper L. Madsen [c], Thomas L. Christiansen [b], Melanie Montgomery [b], John Hald [b]

a College of Mechanical Engineering, Yangzhou University, Yangzhou 225127, PR China

b Department of Mechanical Engineering, Technical University of Denmark, 2800 Kgs. Lyngby, Denmark

c Added Values, Lysholt Allé 8, 7100 Vejle, Denmark

*Corresponding author: Duoli Wu, email: duoliwu@outlook.com, dlwu10s@alum.imr.ac.cn

Abstract

Fireside corrosion is a serious concern in biomass firing power plants such that the efficiency of boilers is limited by high temperature corrosion. Application of protective coatings on superheater tubes is a possible solution to combat fireside corrosion. The current study investigates the corrosion performance of coated tubes compared to uncoated Esshete 1250 and TP347H tubes, which were exposed in two different biomass fired boilers for one year. Data on the fuel used, temperature of the boilers and temperature fluctuations are compared for the two boilers, and how this influences deposit formation, corrosion and the stability of the coatings is discussed. The coatings (Ni and Ni_2Al_3) showed protective behaviour in a wood fired plant where the outlet steam temperature was 520ºC. However, at the plant that fired straw with an outlet steam temperature of 540ºC and where severe thermal cycling took place, both the Ni and Ni_2Al_3 coatings failed. This highlights the differences between the two biomass plants and demonstrates that a coating solution has to be tailored to the operation conditions of a specific boiler.

Keywords: biomass combustion, nickel aluminide coatings, fireside corrosion, power plant testing, operation conditions, metallic materials performance

1. Introduction

As global warming issues are becoming a focus of world attention, there is a strong need to utilize CO_2-neutral fuels in thermal power plants in the future. Biomass is a promising fuel source to reduce greenhouse gas emissions to a near-neutral CO_2 level.[1] However, the high content of potassium and chlorine in deposits formed during combustion of biomass such as straw and grass results in high temperature corrosion on superheaters in the boiler.[2] The KCl-induced high temperature corrosion and related corrosion mechanisms have been extensively investigated in the literature.[2–15] Some studies argue that the corrosion attack initiates with the penetration of Cl species through the oxide scale and results in the formation of metal chlorides. The volatile metal chlorides then diffuse outward and react with O_2 to form metal oxide. The released Cl_2 can then continue this corrosion process and form a cyclic process, which is known as "active oxidation".[12,13] Other investigations reveal that potassium has an active role in accelerating corrosion by leading to the formation of potassium chromate instead of protective Cr-rich oxide.[14,15]

To mitigate biomass corrosion and protect metallic superheater materials, high alloy materials or protective coatings could be applied. Investigation of the reactivity of oxides and KCl has shown that chromium is not effective in providing corrosion resistance as KCl reacts with Cr_2O_3 after 15 hours at 650ºC, however no reaction was observed between Al_2O_3 and KCl.[16] Therefore coatings where Al_2O_3 will form a protective oxide layer such as aluminide coatings are a potential choice to resist KCl-induced high temperature corrosion. However, investigations of the performance of aluminide coatings are seemingly inconclusive. Li and Spiegel investigated the corrosion performance of Fe-Al alloys and a Ni-Al alloy in a KCl-air atmosphere at 650ºC.[17] It was reported that the Ni-Al alloy showed excellent performance, while the Fe-Al alloys experienced extensive corrosion attack. Similar behaviour was reported for exposure beneath a mixed surface deposit of NaCl-KCl in air for 48 h at 670ºC.[18] Kiamehr et al. evaluated the behavior of $Fe_{1-x}Al$, Fe_2Al_5 and Ni_2Al_3 coatings with KCl deposit in air for 168h at 600ºC.[19] After exposure, Ni_2Al_3 coatings showed no sign of attack, while the other coatings were subjected to different degrees of attack. Exposure of Ni_2Al_3 coatings on pure Ni with a small amount of KCl at 600 ºC showed formation of a potassium, aluminium and oxygen rich corrosion product, but the extent of attack was minimal compared to AISI 304 austenitic stainless steel and pure Ni.[20] The investigations by Vokal et al. showed that (Fe,Ni)Al and Ni_2Al_3 coatings were significantly corroded via intergranular and internal chlorination-sulphidation-oxidation, while the Fe_2Al_5 coating was virtually unattacked.[21] This could be due to the fact that this work was performed at 650 ºC where interdiffusion was faster

and the Ni_2Al_3 coating was quickly transformed to NiAl. It is therefore apparent that the actual coating performance depends highly on the exact combination of composition and exposure environment. Pure Ni and electroplated Ni have also resulted in good performance in the laboratory in KCl containing environments,[18] and no reaction has been observed for NiO with KCl.[16,22]

However, all these findings were based on laboratory analysis. For an actual biomass fired power plant, the exposure environment and deposit formation process is much more complex and fluctuating due to factors such as thermal cycling and fuel variability. In-depth investigations of full-scale field exposed components are lacking to elucidate the actual corrosion performance of coatings. The current study addresses the corrosion behaviour of Ni_2Al_3-coated, Ni-coated and reference austenitic superheater tubes, which were all exposed in two different biomass-fired boilers for a year. The corrosion performance of the tubes are compared with respect to the different fuel specifications and the different operating conditions of the two boilers.

2. Material and methods

2.1. Materials and coating manufacturing

Two different austenitic stainless steels, Esshete 1250 and TP347H, were used for the boiler superheater tubes in two Danish biomass fired power plants. The average chemical composition of Esshete 1250 and TP347H are given in Table 1 as specified by SANDVIK data sheets.[23] Sections with a length of 200 mm were cut from these two steel tubes (Esshete 1250: outer diameter (OD) 32 mm, inner diameter (ID) 19 mm; TP347H: OD 33 mm, ID 22 mm).

Table 1. The nominal chemical composition of Esshete 1250 and TP347H (wt. %).

	Cr	Ni	Mn	Nb	Si	C	Mo	V	S	P	B	Fe
Esshete 1250	15	9.5	6.3	1.0	0.5	0.1	1.0	0.3	≤0.015	≤0.035	0.005	Bal.
TP347H	17.5	10	1.7	0.7	0.6	0.05			≤0.015	≤0.030		Bal.

The Ni_2Al_3 coatings were applied to the cut sections of superheater tubes by a two-step process where nickel was first electroplated followed by low temperature pack aluminizing. The samples were grit blasted before the cleaning process was started. The samples were cleaned in anodic degreaser for 3 minutes followed by chemical activation in dry acid for 3 minutes. A pre-plating process was performed in a Woods nickel strike bath (5 minutes with a current density of 6 A/dm^2)

and then a Watts nickel-plating bath was used for the final nickel-plating process. The final plating was performed at 45 °C with a current density of 6 A/dm^2 for 100 minutes. The samples were rinsed in ethanol after processing. The Ni plated tubes were then heat-treated at 650 °C for a period of 1 h in a gas mixture of Ar and 10 vol. % H_2 to strengthen the diffusion bonding between the steel and the nickel layer prior to pack aluminizing.

For aluminizing, the Ni coated tube sections were embedded in pre-mixed pack powders (10 wt. % Al + 8 wt.% $AlCl_3$ + 82 wt.% Al_2O_3), which were put into a cylindrical metal crucible. The crucible was then placed in the tube furnace with flowing argon. The furnace was heated to 650 °C with a heating rate of 18 °C/min, and maintained at this temperature for 6 h. The samples were afterwards cooled inside the furnace by switching off the power while maintaining the argon flow. After aluminizing, the Ni_2Al_3 coated tubes were ultrasonically degreased in acetone and subsequently dried with ethanol. The coating was removed by machining from a 2 cm wide area from both ends of the Ni_2Al_3 coated tubes prior to welding. The tubes after preparation are shown in Figure 1. The discoloration area on the Ni_2Al_3 tubes (Figure 1a) is due to a thin (around 2 μm) Al_2O_3 layer, which was probably related to surface oxidation during furnace cooling or the last part of the pack aluminizing process. Destructive examination from similar locations revealed that the Ni_2Al_3 coating beneath the thin layer was intact and uniform. The bubbles visible on Ni and Ni_2Al_3 tubes (Figure 1b) were probably due to hydrogen gas introduced during the Ni-plating process.

Figure 1. Appearance of the test tubes for (a) Esshete 1250 and (b) TP347H.

2.2. Power plant exposure

The test tubes were welded into a leading superheater tube, where the temperature and therefore corrosion rate was expected to be the highest, at the two different biomass grate-fired combined heat and power (CHP) plants. Randers CHP is located in the central part of Jutland in Denmark and Maribo-Sakskøbing CHP (MSK) is located on the island of Lolland in Denmark. Esshete 1250 tubes were exposed in Randers and TP347H tubes were tested in MSK. The nominal and actual operating conditions of the two plants are shown in Table 2. The test tubes were installed during the yearly overhaul in the summer of 2015, and removed during the summer overhaul in 2016. The exposure time and average steam outlet temperatures are also presented in Table 2. The two plants were chosen to test the coatings because they run with very different operating conditions.

Table 2. The nominal and actual operating conditions of the two plants.

| Nominal conditions	Randers	MSK
Fuel	Wood chips/pellets	Straw/ grass seed chaff
Steam pressure [bar]	110	95
Outlet steam temperature [°C]	520	540
Steam mass flow [kg/s]	29	12.5
Superheater material	Esshete 1250	TP347H
Tube dimensions [mm] OD x wall thickness	31.8 x 6.3	33.7 x 5.6
Superheater design	Vertical hanging	Vertical hanging
Actual operating conditions		
Exposure time [h]	7100 (T_{steam}>450°C)	6200 (T_{steam}>500°C)
Average steam outlet temperature. [°C]	502	536
Average outlet steam temperature where the test tube is installed. [°C]	512	544
Test tube average metal temperature [°C] (bottom-top)	515-518	543-546
Start/stop cycles	1	213

The fuel specifications are different in Randers and MSK, as presented in Table 2. The fuel fired in Randers was composed of 90 wt. % wood chips and 10 wt. % wood pellets, while 79 wt. % wheat straw and 21 wt. % grass seed chaff was fired in MSK. Wood chips and wheat straws are the most abundant biomass resources in Denmark. A general overview of the major chemical elements

present in the biomass utilized in Randers and MSK is shown in Table 3. The chemical compositions from Randers were actual measurements of the fuel used at the plant in 2012,[24] whereas those for MSK were taken from the ECN database for wheat straw and grass seed chaff.[25] The chemical compositions were measured on dry basis and the overall values were calculated based on the percentage of different biomass resources used.
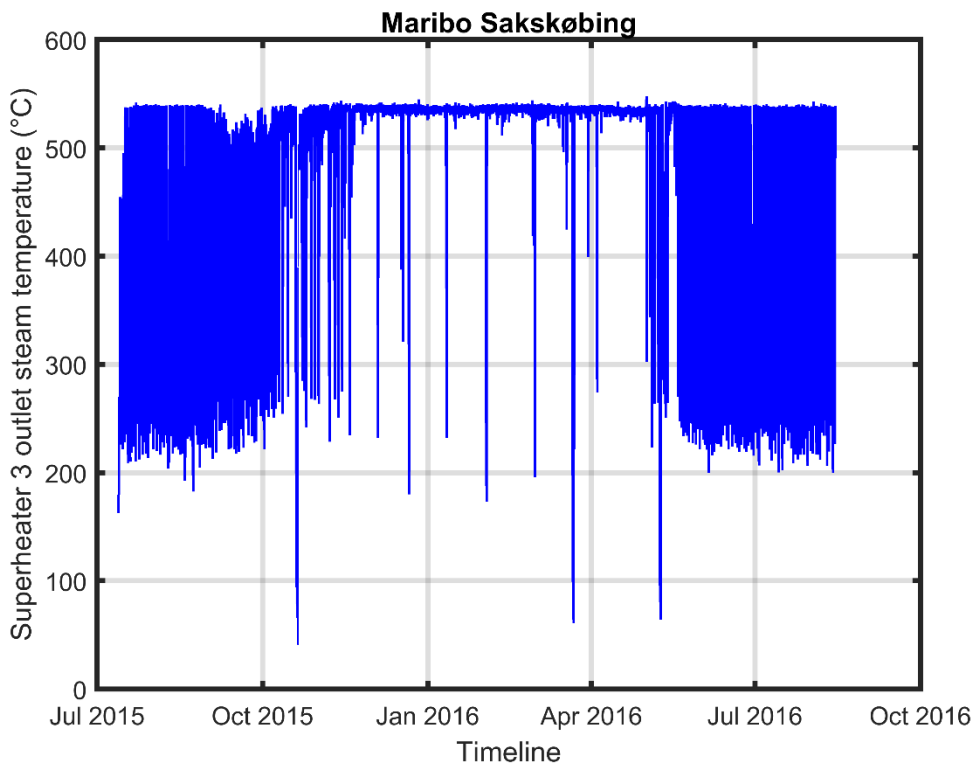
Table 3. Fuel data for Randers and MSK.

Power Plants	Randers			MSK		
Biomass resources	Wood chips	Pellets	Overall value	Wheat straw	Grass seed chaff	Overall value
Moisture, wt.%	6.50	6.25	6.48	8.70	11.24	9.23
Ash, wt.%	0.80	3.82	1.10	2.80	13.38	5.02
Chlorine, Cl, wt.%	0.02	0.06	0.02	0.23	0.14	0.21
Sulphur, S, wt.%	0.01	0.09	0.02	0.15	0.18	0.16
Carbon, C, wt.%	49.60	47.68	49.41	47.79	41.33	46.43
Hydrogen, H, wt.%	6.00	6.05	6.00	5.91	5.49	5.82
Nitrogen, N, wt.%	0.17	1.11	0.26	0.68	1.69	0.89
Oxygen, O, wt.%	43.00	41.17	42.82	42.07	37.79	41.17
Potassium, K, wt.%	0.10	0.66	0.15	0.98	0.71	0.92

The operating conditions for the two CHP plants are also different. At Randers it is preferred to run at part load rather than shutting the plant down when the heat demand is low, and as shown in Figure 2, has only had one shutdown during the exposure period. However, at MSK the plant is run under cyclic conditions with daily start/stops in the beginning and end of the heating season (Figures 3 and 4). This means that at MSK the boiler runs at full load when in operation. This difference in operating conditions can also be seen when comparing the temperature histograms, which is broad for the Randers plant, and narrow for the MSK plant (Figure 5).
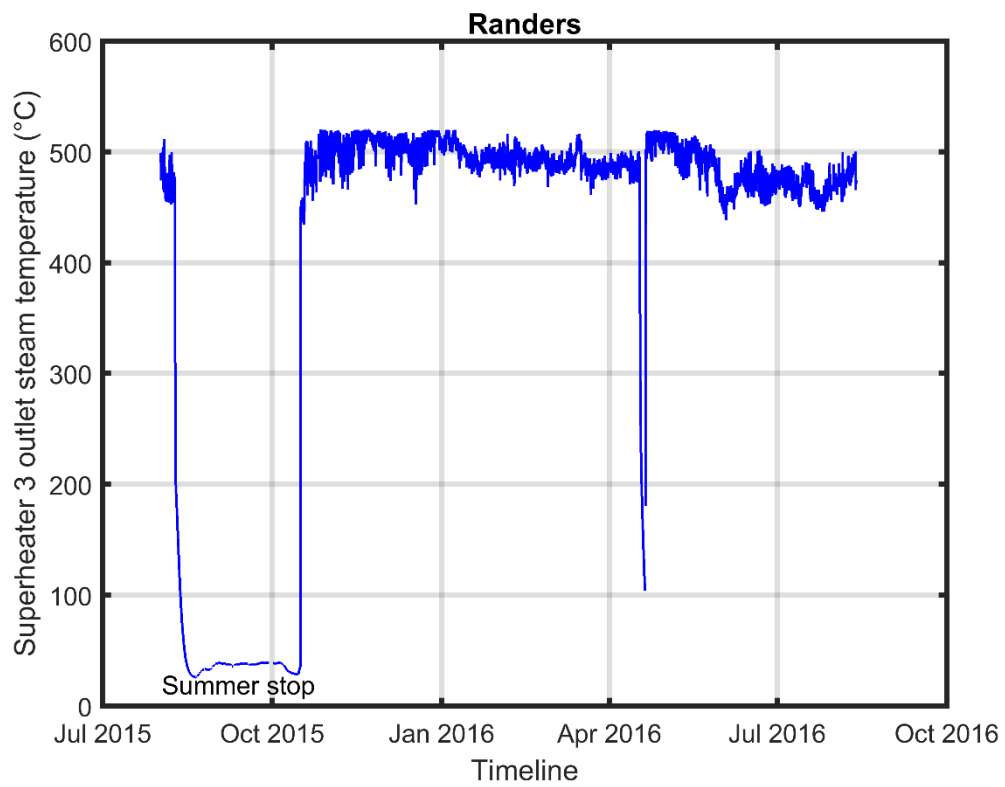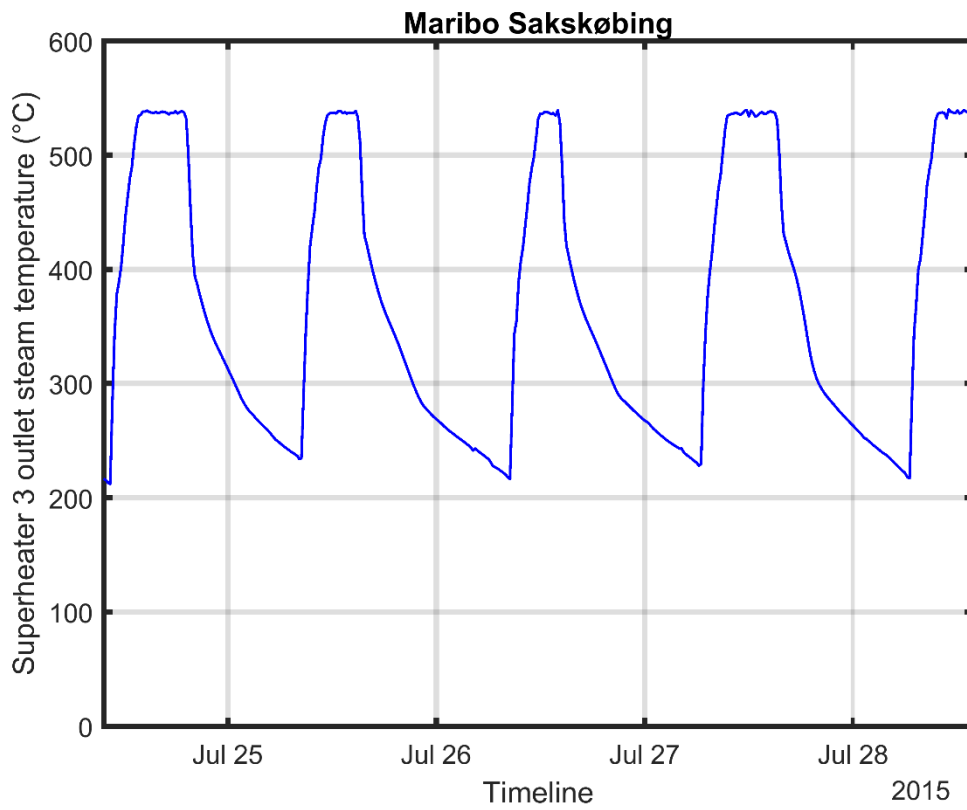
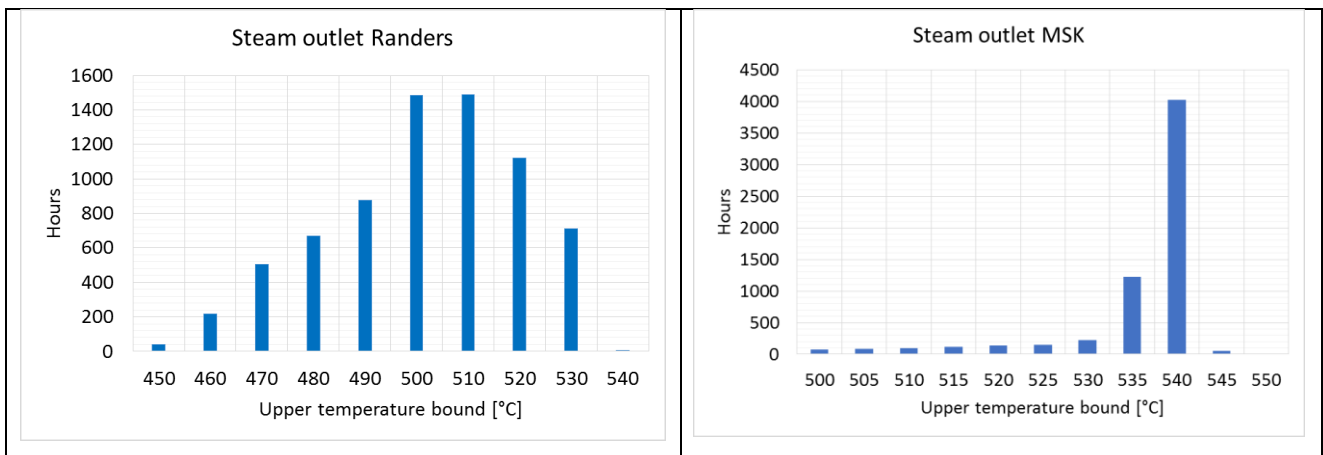**Figure 2.** The outlet steam temperature data for the exposure period in Randers.

**Figure 3.** The outlet steam temperature data for the exposure period in MSK.

Figure 4. The outlet steam temperature data showing the daily cycle in MSK.


Figure 5. Temperature histograms for Randers and MSK.

2.2.1. Randers test tube

A cross-section of the Randers boiler, as well as superheater 3 (SH3) with the test tube is shown in Figure 6. SH3 has 14 parallel tube banks and the test tube was placed in bank no. 8, close to the centre of the boiler. The position of the test tube was chosen based on temperature analysis of the superheater with considerations to geometrical limitations. The temperature analysis was performed using a numerical tube model where the tube internal and external metal temperatures are calculated from inlet to outlet, under given boundary conditions (inlet/outlet steam temperature, steamside oxide thickness, material properties, heat flux profile, pressure, etc.).[26] The oxide thickness is calculated in the model as a simulation from new to actual time of operation. The oxide growth kinetics is based on tube investigations from other plants with the same materials. A bimodal flux profile was assumed for the Randers analysis, due to the double pass of the SH tubes. The heat flux is assumed to be the highest near the bottom (closest to the grate) and the lowest at the boiler roof. The resulting temperature profile from inlet to outlet at a steam outlet temperature of 512°C is shown in Figure 7. The metal temperature, which controls the corrosion process, is the highest in the high flux areas, and peaks around 19 m from the inlet (with the chosen flux profile). The test tube was placed 18-20 m from the inlet as indicated in Figure 6, i.e. at the peak metal temperature. The position is easy to access and the tube outlet temperature is measured with a thermocouple.
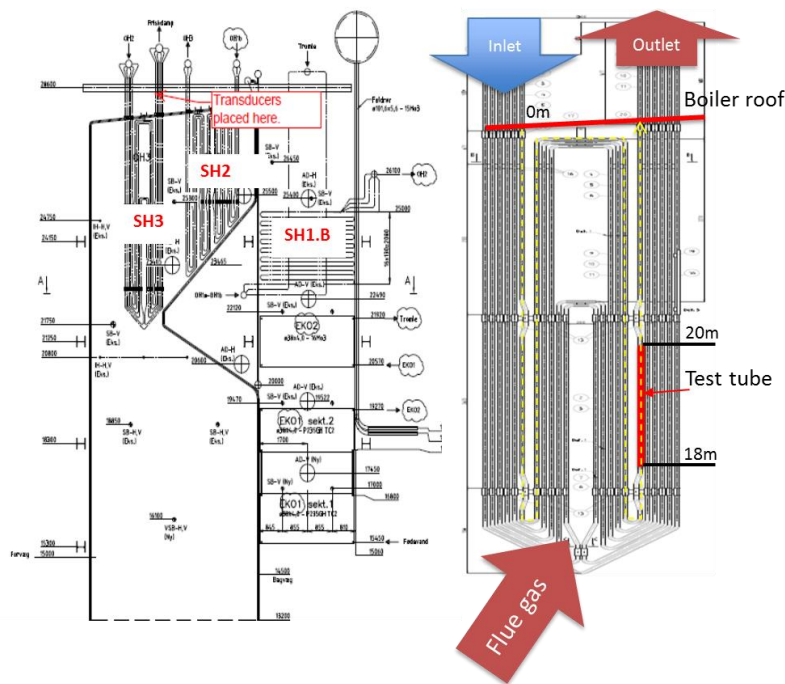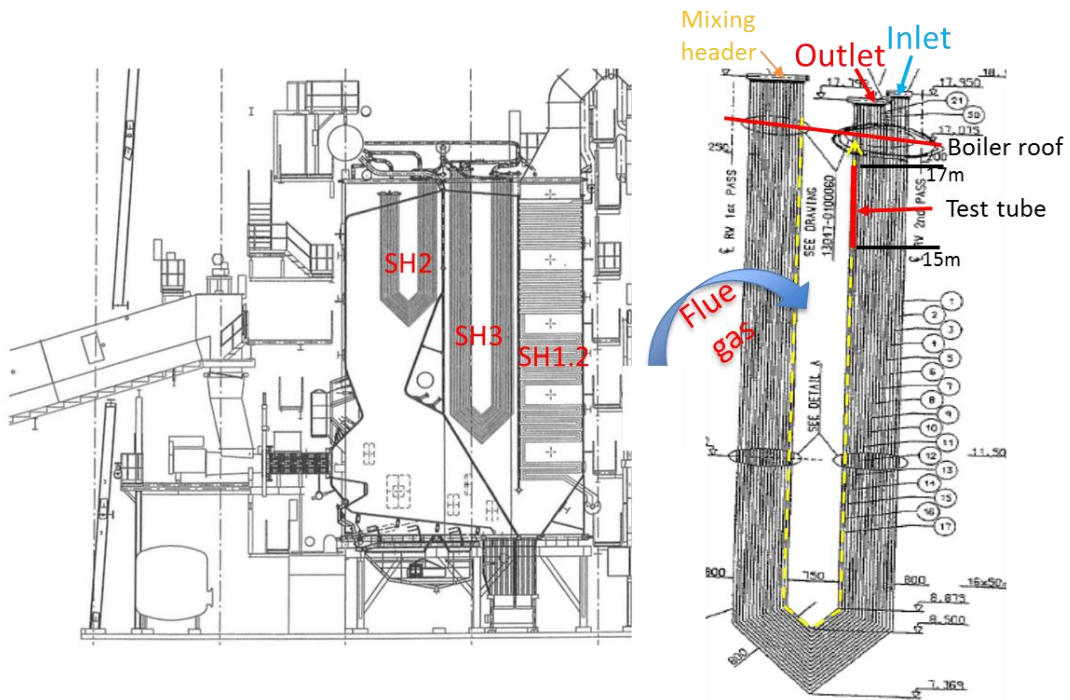

Figure 6. Cross-section of Randers boiler and position of the test tube on superheater 3.
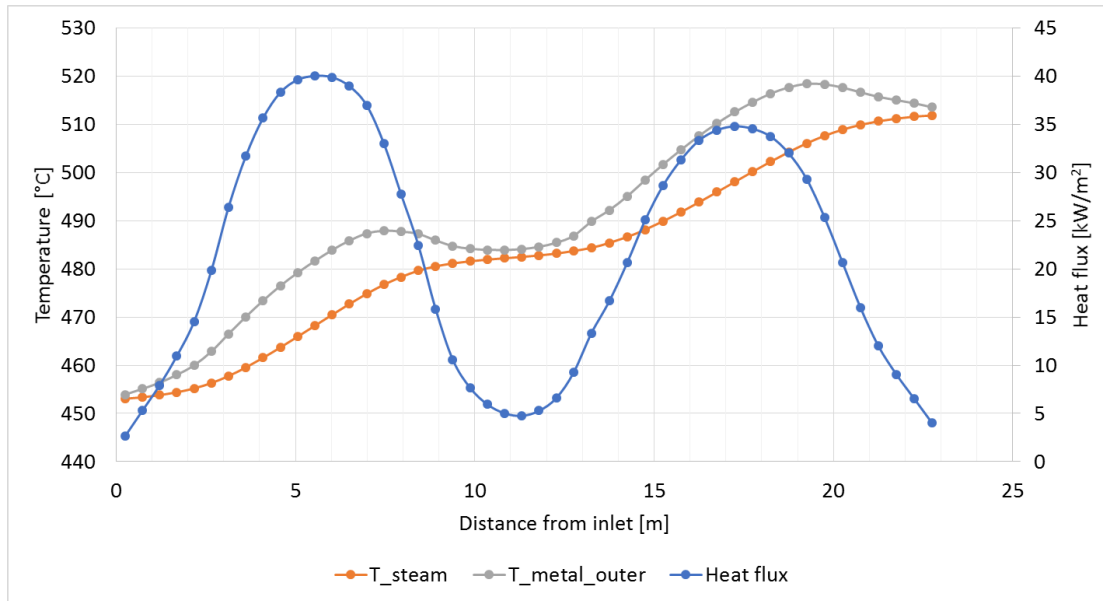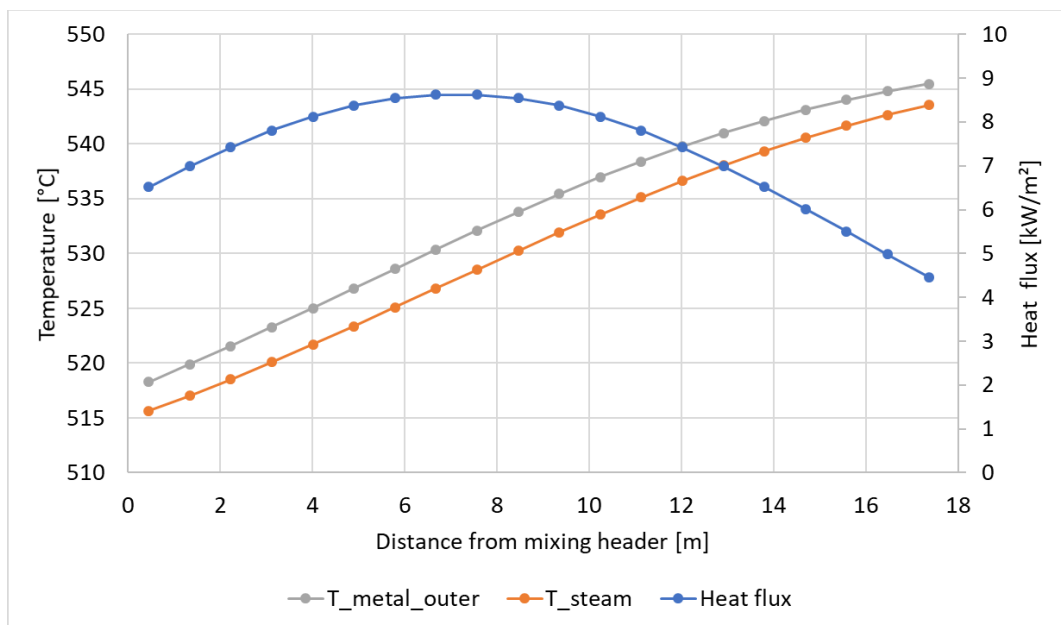
Figure 7. Calculated steam and outer metal temperature of SH tube from inlet to outlet in Randers. The test tube was placed from 18-20 m from the inlet.

2.2.2. MSK test tube

In Figure 8, a cross section of the MSK boiler and superheater 3 (SH3) is shown. At MSK, SH3 is placed in the second pass of the boiler as indicated. SH3 has 8 parallel tube banks and the test tube is placed in bank no. 4, close to the centre of the boiler. The position of the test tube was chosen in the same way as in Randers. For MSK a parabolic heat flux was chosen. This profile was chosen based on the assumption that the heat flux (flue gas flow and temperature) is slightly higher near the nose of the boiler compared to the boiler roof. The results of the temperature analysis are shown in Figure 9. Due to the lower overall heat input, and lower steam mass flow, the average heat flux is lower at MSK than in Randers. With the chosen flux profile, the outer metal temperature is almost parallel to the steam temperature and reaches the highest value at the superheater outlet. The test tube was placed close to the outlet, approximately 0.4 m under the boiler roof. This area is also reported from the plant operator to have high corrosion rates. Analysis of temperature measurements from tubes adjacent the test tube indicates that the steam temperature is approximately 8°C above the average steam temperature. Therefore, 8°C has been added to the average steam temperature in this analysis (see Table 2).

Figure 8. Cross-section of MSK boiler and position of the test tube on superheater 3.

Figure 9. Calculated steam and outer metal temperature of SH tube from mixing header to outlet in MSK. The test tube was placed from 15-17 m close to the outlet.

2.3. Sample preparation and characterization

After plant exposure, the test tubes were removed from the Randers and MSK boilers. The tube sections were cut into thin rings (1 cm) in dry condition and were embedded in epoxy resin. In order to reduce dissolution of water-soluble compounds, grinding and polishing were performed using absolute ethanol as lubricant. Grinding was performed using SiC paper, while polishing was done with diamond slurry until a final step of 1 μm diamond. The cross-sections were examined using a scanning electron microscope (FEI Inspect S) equipped with energy dispersive X-ray Spectroscopy (Oxford Instruments 50mm^2 X-Max silicon drift detector) for chemical analysis (SEM-EDX). A JEOL JSM-5900 Scanning Electron Microscope (SEM) with Energy Dispersive Spectrometer (EDS) was also applied. The acceleration voltage of 15kV and high beam current was used. Image acquisition was performed both in secondary electron (SE) mode and back-scattered electron (BSE) mode with high vacuum. Deposits from both tubes were photographed using an Olympus BH-2 stereomicroscope. The deposits were prepared in cross-sections by dry polishing up to 4000 grit paper, and investigated with scanning electron microscopy. In addition the surface of deposits adjacent the tube were examined with SEM-EDX. The residual metal thickness was measured with Olympus BH-2 stereomicroscope. The metal loss was calculated based on the original tube/coating thickness and measured residual metal thickness. The average corrosion rate then was calculated with metal loss divided by total exposure time.

3. Results and discussion

3.1. Ni and Ni$_2$Al$_3$ coatings before exposure

A cross sectional view of the Ni and Ni$_2$Al$_3$ coated samples are shown in Figure 10. The Ni coating consisted of a single Ni layer with a thickness of 135($\pm$5) μm. The Ni$_2$Al$_3$ coating, with a double layer structure, was adherent to the steel. The double layer coating consisted of an outer Ni$_2$Al$_3$ layer (thickness variation between 50 and 70 μm) and an inner Ni layer (100μm).

Few small porosities could be observed locally at the Ni/steel interface, which indicates a good quality of the Ni deposition process. The presence of Ni$_2$Al$_3$ phase was confirmed by XRD (not shown). From the thermodynamic point of view, any stable phase at 650°C within the Al-Ni binary phase diagram can form during the coating preparation process. In practice, however, kinetics play a large role and only Ni$_2$Al$_3$ was observed directly after the low temperature aluminizing process. The reason is that the interdiffusion coefficient for Ni$_2$Al$_3$ is at least two orders of magnitude higher than for the other nickel aluminides.[27]
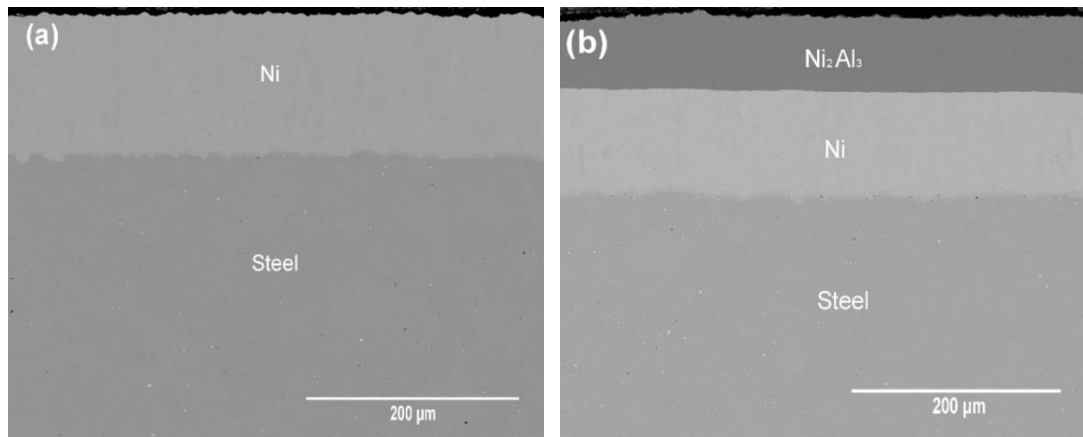
Figure 10. BSE micrograph of the as coated samples for (a) Ni coated and (b) Ni_2Al_3 coated.

3.2. Deposit composition on test tubes

The deposits were removed from the exposed tubes and examined with SEM-EDX. The deposit from Randers was sintered to the tube and a scalpel was required for removal whilst the deposit from MSK was fragile and easily flaked off. Photographs of the deposits are shown in Figure 11. The deposit from Randers was more compact with different layers where a whitish layer was present adjacent the tube. When the deposit was removed from the tube, almost no oxide was adherent. The deposit from MSK consisted of white crystals adherent to the underlying oxide and on the coated tube. Some of the coating was also present within the deposit. Analysis of this spalled coating is described in our previous work.[28]
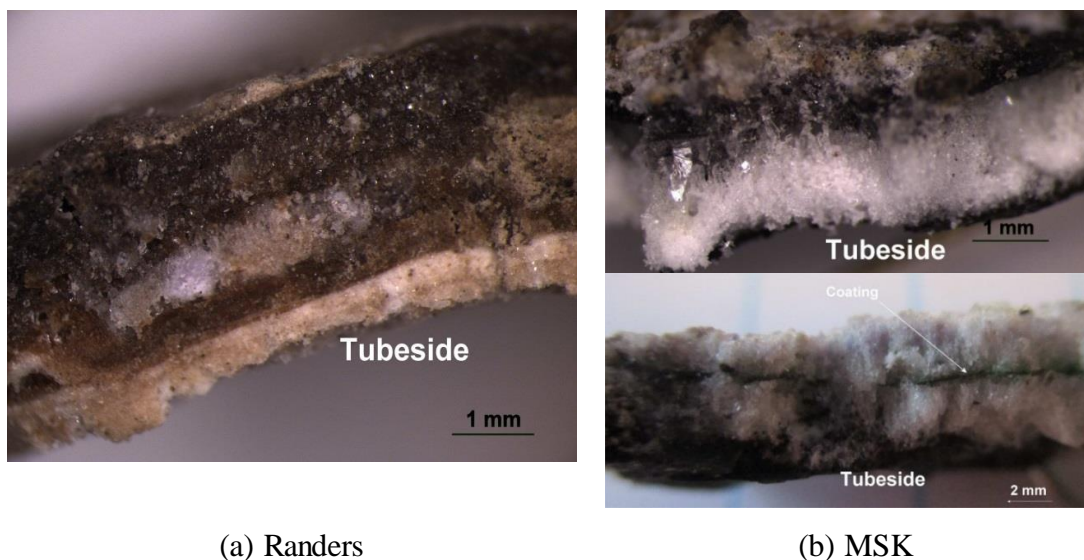

(a) Randers   (b) MSK

Figure 11. Appearance of deposit removed from the exposed tubes (a) deposit from Randers power plant, (b) deposit from MSK power plant.

The surface morphology and composition of the deposit close to the tube was investigated using SEM-EDX on both deposit flakes and cross-sectioned deposits. For deposit from Randers, the analysis of the underside of the deposit revealed two different morphologies (Figure 12a), a smooth morphology, which was probably KCl as the measured mole ratio for K/Cl was 1:1, and small particles that were presumably sulphates of potassium and calcium. Analysis of the dry polished cross-sections of the deposit also detected K, S, Ca and O and K, Cl rich regions (Figure 12b). These elements were present throughout the deposit, however there were more Si rich particles on the outer part of the deposit.
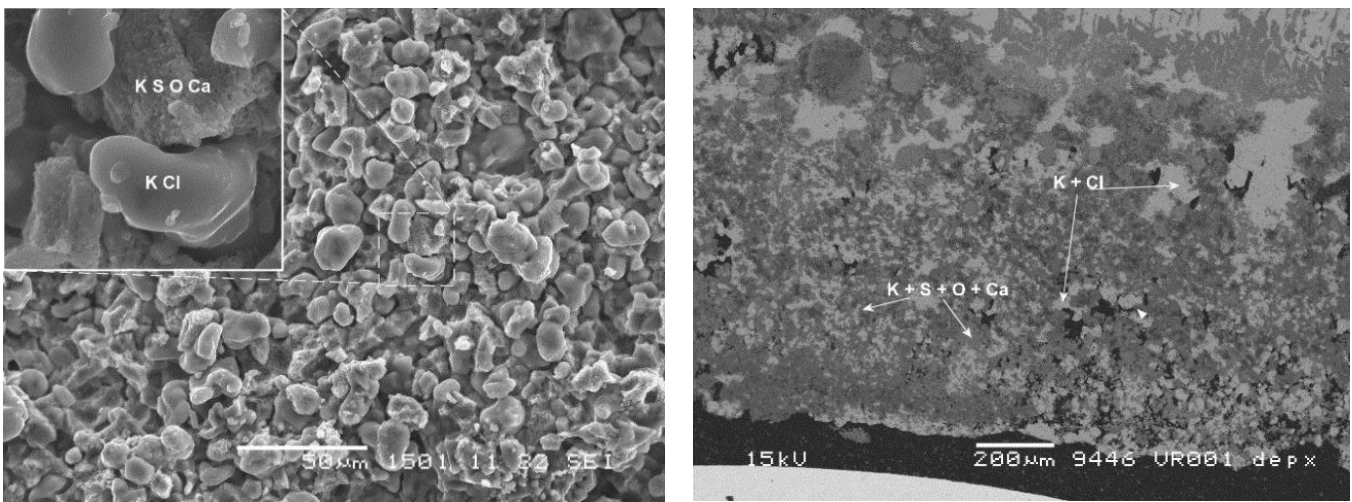
(a) Deposit adjacent to tube   (b) Cross-section of deposit

Figure 12. SE micrograph of surface morphology and BSE micrograph showing the composition of deposit from Randers (a) deposit adjacent to tube, (b) Cross-section of deposit.

Facetted cubic structures were typical on the unprepared deposit from MSK (Figure 13a), where the cubic structures had a composition corresponding to KCl. The KCl was in direct contact with the surface oxide and there were remnants of iron oxides on the surface. Cross sections of the dry polished deposit also showed that KCl is present adjacent to the oxide surface and there was only occasionally K, S, and O (presumably potassium sulphate) present (Figure 13b).
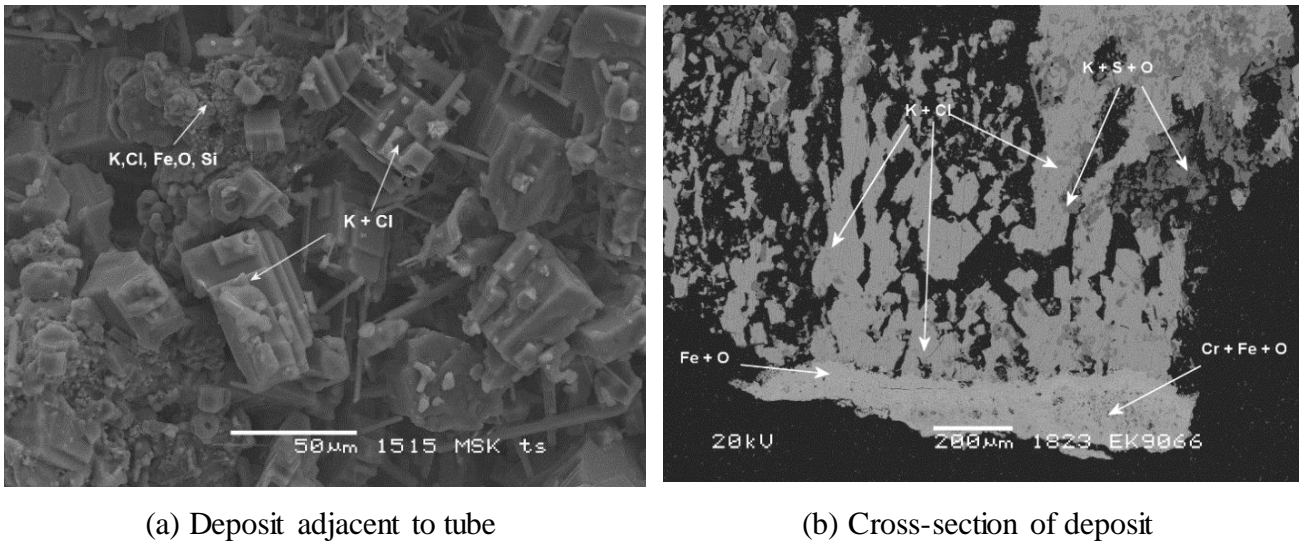
(a) Deposit adjacent to tube   (b) Cross-section of deposit

Figure 13. SE micrograph of surface morphology and BSE micrograph showing the composition of deposit from MSK (a) deposit adjacent to tube, (b) Cross-section of deposit.

The high K and Cl content in the deposit adjacent the tube at MSK and Randers is due to the fuel used which was rich in potassium and chlorine (see section 2.2.). Since only small amounts of potassium sulphate were present adjacent the deposit at MSK, this would indicate that the sulphation process of KCl only has a partial contribution to the corrosion attack compared to Randers. In laboratory experiments, Okoro et al. measured similar extents of internal corrosion attack for specimens in an oxidizing environment ($CO_2+H_2O+O_2$) with and without $SO_2 + HCl$, as long as KCl was present.[29] The different morphologies of the KCl deposits may be linked to the tube temperature difference, which is lower at Randers than at MSK. Bröstrom et al. investigated condensation of KCl and showed that above 500ºC,[30] facetted KCl crystals were formed similar to Fig. 13a whereas at lower temperatures, a more dendritic appearance was apparent. They suggested that vapor is cooled by thermal conduction from the metal tube, and then outward growth occurs by direct condensation of vapor phase to result in this structure.

At MSK, there were many thermal cycles and this could contribute to repeated spallation of the deposit resulting in new deposit forming on the tube. In contrast, the more sintered deposit from Randers may be more protective against incoming corrosive species. It could be suggested that after the initially formed KCl is exhausted, corrosion would decrease, as it would be more difficult for KCl to advance to the surface of the tube resulting in corrosion. Lindberg et al. describes the behavior of a deposit due to a thermal gradient at deposit/flue gas interface, revealing how deposit can be vaporized from the flue gas-deposit surface, and species can be transported and condensed

throughout the underlying deposit, thus resulting in KCl being "transported" through a deposit with longer exposure times resulting in more KCl being transported from deposit to steel surface.[31] This would explain why KCl is present on the underside of the deposit. Cubic facetted KCl particles similar to those observed in the deposit from MSK were observed with TEM when SO_2 was not present in a gas stream in laboratory testing,[32] otherwise KCl condenses on the potassium sulphate particles in the gas phase and then deposit on surfaces, which could be what has occurred at Randers.

During biomass combustion, potassium is present as KCl whilst sulphur is present as SO_2. When the temperature decreases below 1000ºC this will lead to oxidation of SO_2 to SO_3 and the sulphation of KCl to K_2SO_4, thus not only the presence of SO_2 but flue gas temperature will decide whether sulphation occurs.[33] With the limited information about the flue gas temperature and composition in the two different biomass fired plants, it is unclear whether the morphology of the KCl can be linked to the Cl:S ratio, the temperature gradient or other factors such as flue gas temperature changes. However the different morphologies and KCl abundance adjacent the tube reveals different environments around the tubes in the two plants which could have influence on the performance of the tested coatings.

3.3. Ni_2Al_3 coatings, Ni coatings and reference tubes after exposure

3.3.1 Microscopy analysis of uncoated tubes

The corrosion morphology of the exposed uncoated tubes from Randers (Esshete 1250) and MSK (TP347H) are similar. The corrosion morphologies consist of a porous outer oxide, an inner selective corrosion area and grain boundary attack (Figure 14). The oxide located in the outermost corrosion product was rich in chromium and iron, while the oxide beneath was rich in nickel. No indications of formation of a protective chromium-rich oxide could be seen. This type of corrosion morphology is typical for chlorine induced corrosion, where volatile metal chlorides form via reaction of metal with chlorine species. As metal chlorides are transported towards the outer surface they react with oxygen to form the porous outer oxide while the chlorine is released to again react and form new volatile metal chlorides, a chlorine corrosion cycle that is often referred to as active oxidation.[2] Because of the progression of the corrosion attack it is unclear if an initial breakdown of protective oxide scale occurred due to potassium chromate formation from a chemical reaction

between chromium rich oxide and KCl as shown in laboratory studies or whether corrosive chlorine species could enter into the steel/oxide interface along pores or cracks in the oxide.[16,30,31]
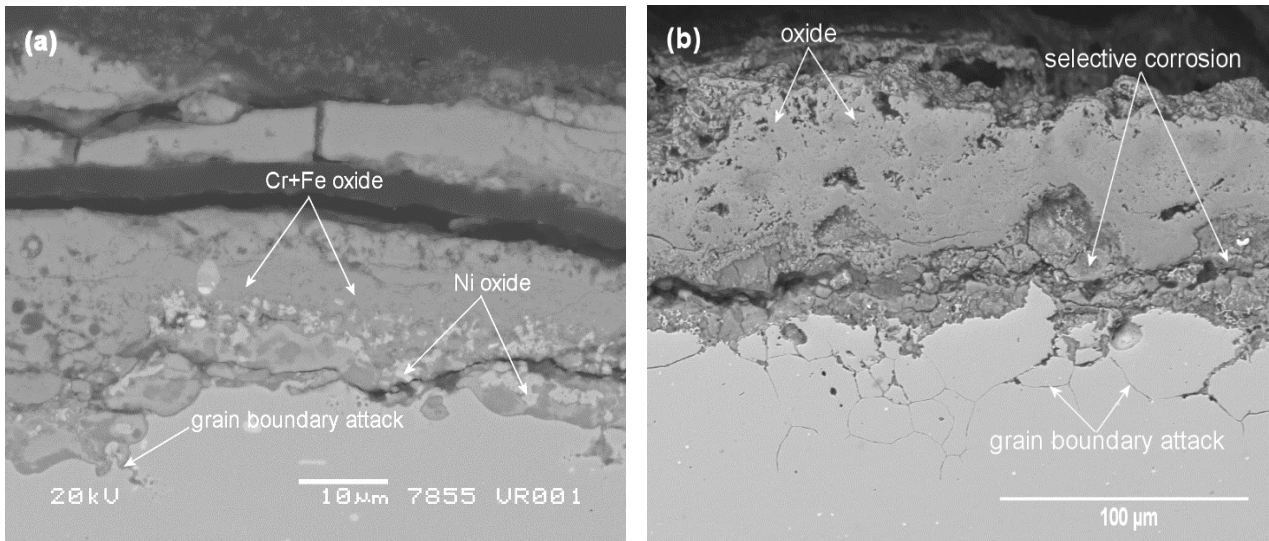
Figure 14. Corrosion morphology on uncoated tubes after boiler exposure in (a) Randers and (b) MSK.

After exposure, the actual metal loss for the non-coated steel was measured for both plants. The corrosion rate was then calculated based on the measured metal loss and the total exposure time (Table 4), which clearly reveals that the corrosion in the MSK plant is much more aggressive than at Randers. For the exposure in MSK, the average metal loss and corrosion rate are almost 30 times higher than Randers.

Table 4. Average metal loss and corrosion rate for Randers and MSK

Power plant	Randers	MSK
Average metal loss (µm)	23(±8)	651(±139)
Average corrosion rate (µm/1000h)	3	105

3.3.2 Microscopy analysis of Ni coated tubes

The corrosion morphology of the exposed Ni coated tubes for Randers and MSK are very different as shown in Figure 15. The Ni coated tube showed good performance after exposure in Randers where the Ni layer was still attached to the steel and no significant attack was measured. The measured metal loss is 3.37($\pm$2.25) μm and the calculated corrosion rate for Ni is 0.47 μm/1000h. Similar results have been observed in the laboratory. Ni revealed a significantly better performance compared to Fe-Cr-Al alloys at 670ºC with KCl in air, but had lower performance compared to NiAl alloys.[18] When two different exposures were conducted at 600ºC with slightly different oxidising gases and with and without KCl, a nickel oxide of 4 μm was formed in both exposures even though the amount of KCl was much higher in one of the experiments.[16] However, for the exposure in MSK, severe attack occurred and the 135μm thick Ni layer was no longer present. The corroded tube section had a mixed iron and chromium oxide at the surface and grain boundary attack into the substrate steel, which was similar to the corrosion morphology observed on the uncoated tube. It is highly probable that the slight mismatch in thermal expansion coefficients gives problems where there is excessive thermal cycling at MSK. Thus cracks/channels can form that allow for the migration of corrosive species to the Ni-steel interface and the outward migration of Cr chlorides.[28] The corrosion attack thus occurring underneath the Ni-layer will further contribute to poor adhesion between Ni-layer and steel tube.
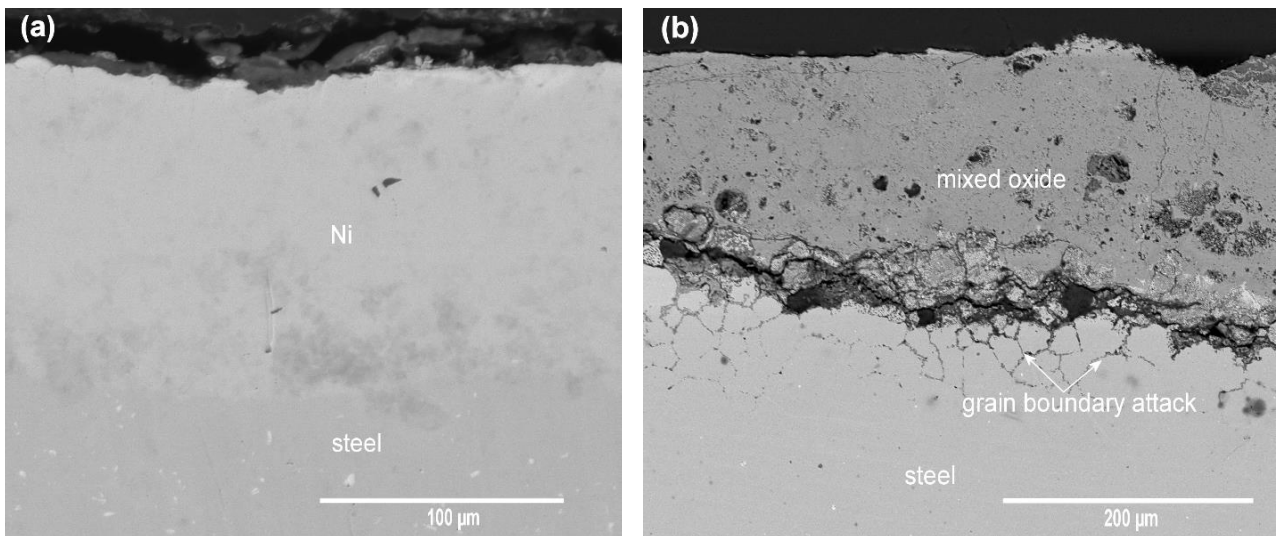
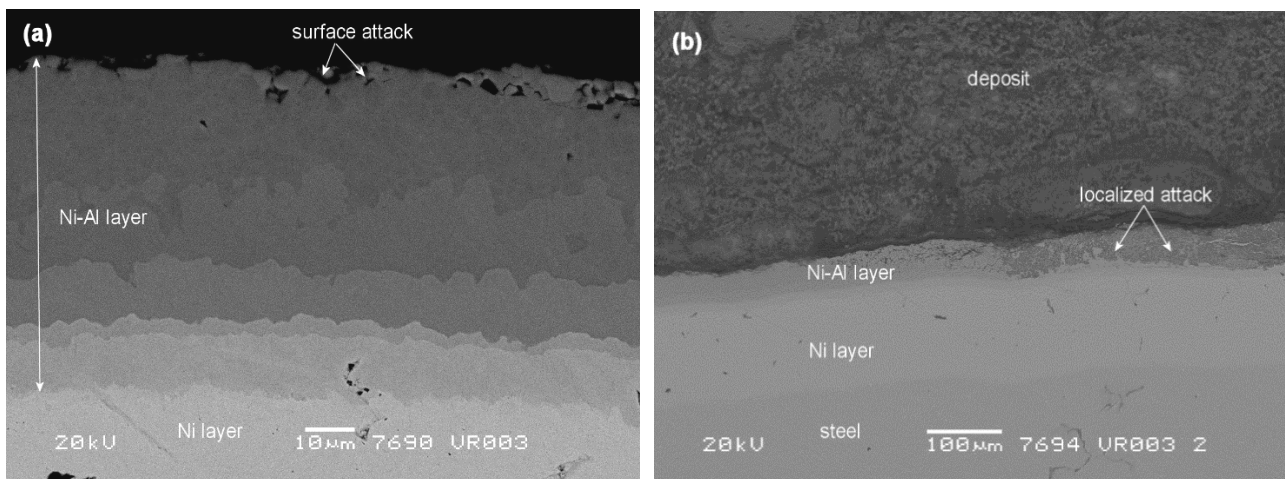**Figure 15.** Corrosion morphology on Ni coated tubes after boiler exposure in (a) Randers and (b) MSK

3.3.3 Microscopy analysis of Ni₂Al₃ coated tubes

Exposure in Randers

The Ni₂Al₃ coated tube showed good high temperature corrosion performance after testing in the Randers boiler. In most places (4/5 of the observation area), the Ni₂Al₃ coating showed protective behaviour with only slight surface attack (Figure 16a). In localized areas (1/5 of the observation area), the Ni₂Al₃ coating was attacked and Al depletion was visible. However, the coating attack ended above the Ni layer and no further penetration was observed (Figure 16b). At all locations, the underlying steel was well protected without sign of corrosion attack. Compared to the as-coated condition shown in Figure 10, some interdiffusion between the Ni₂Al₃ layer and the Ni layer is observed, resulting in formation of other phases from the Ni-Al phase diagram at the interface.

Figure 16. Corrosion morphology on Ni₂Al₃ coated tube after boiler exposure in Randers. (a) general protective area, (b) localized attack area.

The coating thickness was measured after exposure in 12 positions clockwise around the circumference of the Ni₂Al₃ coated tube as shown in Figure 17 where 12:00 is the flue gas direction. The coating thickness around the Ni₂Al₃ coated tube is asymmetric. The deposit growth is typically asymmetric around a superheater tube depending on the flue gas flow conditions that vary around the tube. The attack at areas opposite the flue gas may be due to the varying deposit parameters on the upstream (12:00) compared with the downstream (06:00) part of the tube.[34]
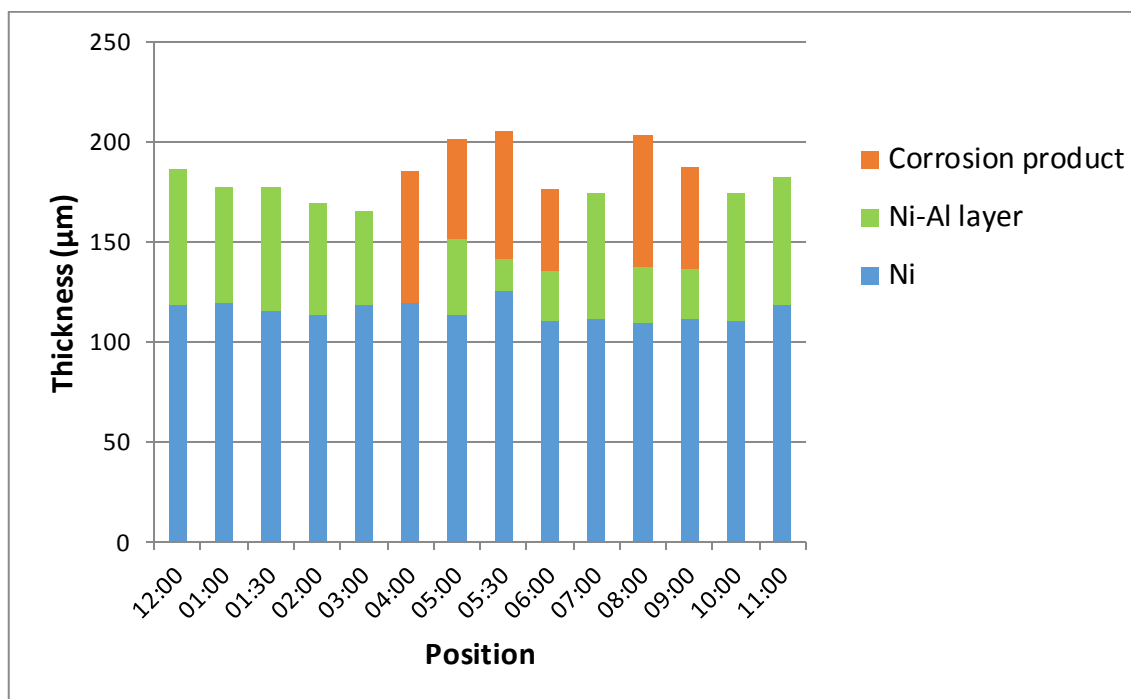
Figure 17. Residual thickness of layers around the circumference of the Ni_2Al_3 coated tube in Randers.

Compared with Ni, Fe and Cr, Al has the highest affinity for reaction with both chlorine and oxygen. Presumably, aluminium chloride can form at the deposit/Ni_2Al_3 coating interface when the oxide partial pressure is low. Because of the low melting point of aluminium chloride (192 °C), aluminium chloride will volatilize and migrate outwards rapidly.[18] The volatilized aluminium chloride will be transformed into aluminium oxide where the oxygen partial pressure is higher, leaving behind a depleted or porous area. Li et al. saw rapid early stage volatilization when exposing Fe-Al alloys and a NiAl alloy to NaCl-KCl melts at 670 °C but observed that the attack slowed down when a thicker alumina layer was established on the surface.[18] This agrees well with the corrosion morphology observed on the Ni_2Al_3 coated tube in Figure 16a. The surface attack of the Ni_2Al_3 coating indicates that an initial corrosion attack has happened, while a continued attack did not occur. However, in some locations (localized attack in Figure 16b), there was no slowing down when attack was initiated. Some studies have argued that this type of attack can be due to a chemical reaction between alumina and gaseous KCl where the flue gas temperature is high, which can break down the protective alumina.[19] According to the investigations by Pettersson et al.,[35] gradual volatilization of KCl would occur at temperatures above 560°C, where the vapour pressure of KCl exceeds 10^{-6} atm. With the breakdown of the protective Al_2O_3, the corrosion process could proceed and a porous Al-depleted layer would develop underneath the surface (Figure 16b).

Exposure in MSK

Compared with the exposure in Randers, the Ni_2Al_3 coated tube performed much worse in MSK. As shown in Figure 18, the nickel aluminide layer was no longer adherent to the tube; this was the case around the whole tube circumference. The spalled nickel aluminide coating could be found within the deposit, and investigations showed that in the spalled section some Al depletion had occurred but there was still alumina. This was documented in detail in previous work.[28] Remnants of an oxidized nickel layer (up to 70 µm) were present in approximately two-thirds of the circumference of the tube sample with varying depths of attack of the underlying tube. This indicates that the Ni_2Al_3 layer offered some initial protection before spalling off, since there was no Ni left on the tube coated only with Ni (cf. Fig. 15b). The previous investigation showed that the presence of a Ni_2Al_3 coating hinders evaporation of metal chlorides from the corrosion front, but does not prevent Cl species diffusing to the corrosion front. Beneath the Ni layer, the formation of trapped nickel chloride also hampered the corrosion process by binding the aggressive chlorine.[28]
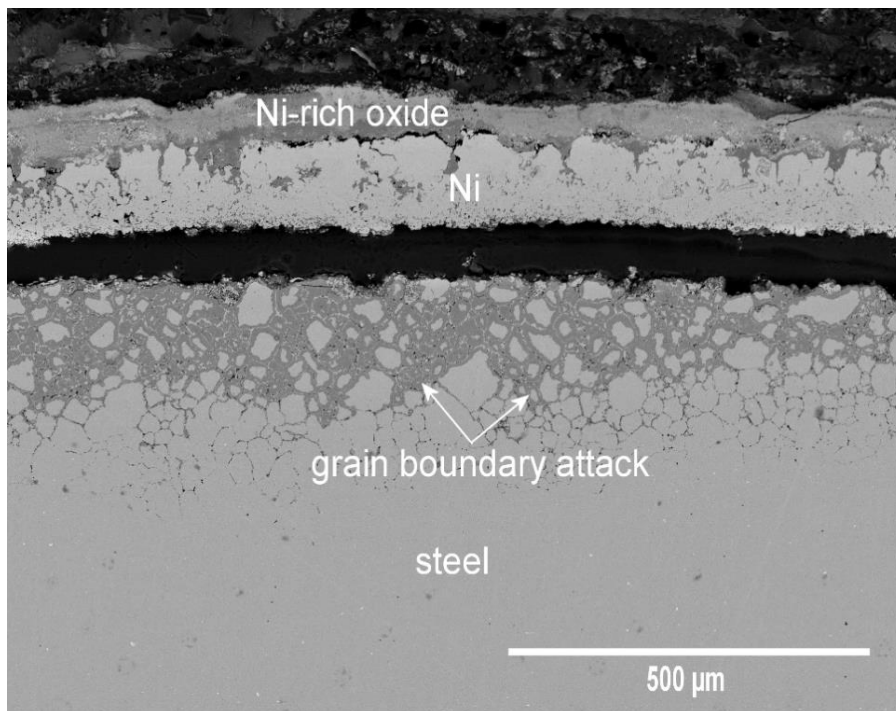
Figure 18. BSE image of corrosion morphology for the Ni_2Al_3 coated tube after boiler exposure in MSK

Since there are many thermal cycles at MSK (Figures 3 and 4), the most probable explanation for the spallation of the Ni_2Al_3 coating lies in the difference in thermal expansion coefficients between the steel, Ni, Ni-Al intermetallics forming at the interface and the Ni_2Al_3. The coefficients of thermal expansion (CTE) for the steels, Ni, NiAl and Ni_2Al_3 are depicted in Figure 19. For the

power plant exposure temperature interval between 300°C and 600°C as shown in Figures 3 and 4, the CTE for Ni_2Al_3 differs significantly from the CTE for Ni, NiAl and steels. A full stress analysis is outside of the scope of the present paper, however, as the CTE for Ni_2Al_3 and Ni are quite different, thermal stresses could be expected which would lead to the spallation of the Ni_2Al_3 coating in MSK. The spallation of Ni from the steel was probably related to the corrosion attack of the underlying steel which led to a weak adhesion between Ni and steel.
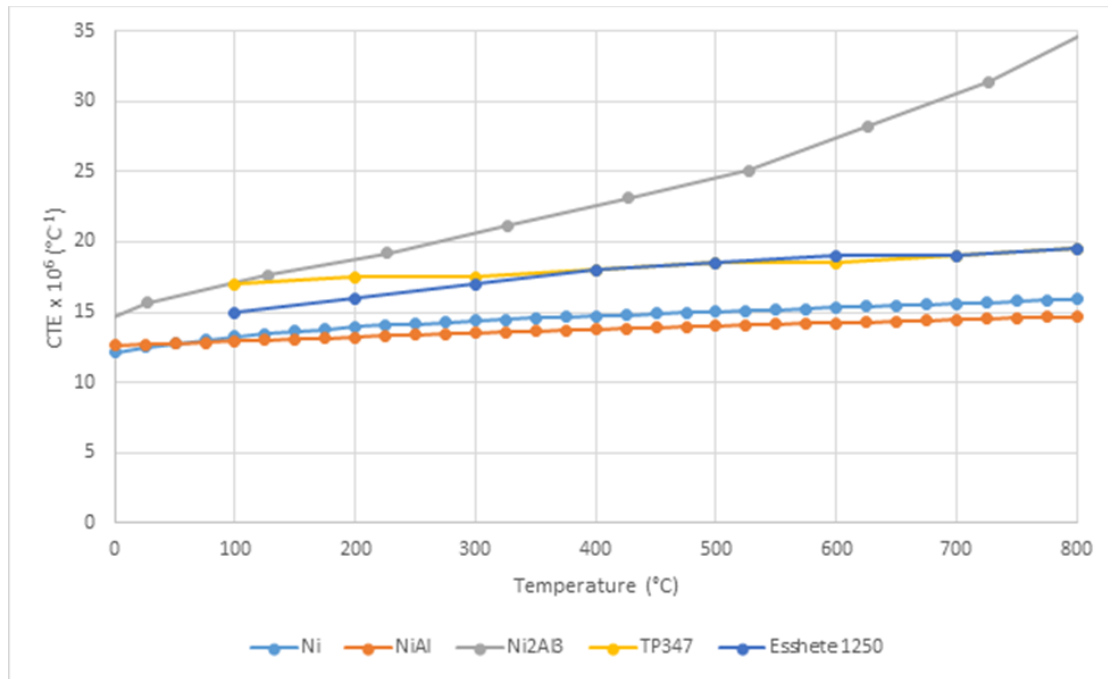
Figure 19. The variation of CTE with temperature of pure Ni, NiAl, Ni_2Al_3, TP347H and Esshete 1250.[36,37]

3.4. Comparison of coating performance depending on plant

Based on the above discussions, it clearly demonstrates that the applied Ni and Ni_2Al_3 coatings show very different corrosion performance in the different biomass fired power plants. In the Randers plant, both the Ni and Ni_2Al_3 coatings showed protective behaviour, while the coatings spalled off when exposed in MSK. The fuel utilized, operation temperatures and temperature cycling characteristics differ hugely between the two plants as do the corrosion rates. These are critical factors that play a key role in the observed coating performance.

3.4.1. Fuel comparison

According to Table 3, there are clear differences between the fuel data for the two plants, Randers and MSK. Most important is that the content of potassium and chlorine in MSK is much higher than in Randers. It is widely accepted that fireside corrosion is mainly induced by a high content of

potassium and chlorine from the biomass fuel.[2] Besides the content of potassium and chlorine, the sulphur to chlorine ratio also plays an important role for superheater corrosion.[13,38] The investigation by Krause et al. showed that the corrosion problem is significantly reduced when the sulphur to chlorine mole ratio (S/Cl) in biomass fuel is high i.e. 4.[38] Grabke et al. also reported a similar tendency in their study.[13] It has been suggested that the best way to prevent corrosion during biomass firing is to keep the S/Cl molar ratio in the fuel higher than 2.0 and preferably higher than 4.0.[39] For our exposure studies, the S/Cl molar ratio in Randers was 1.10, while in MSK it was 0.84 so that corrosion due to KCl would be expected in both cases. The differences in S/Cl ratio are consistent with the analysis of the deposits (section 3.2). Larger amounts of potassium sulphate were present within the deposit adjacent the tubes in Randers than in MSK. The sulphation process of deposited KCl can also affect the corrosion attack; the sulphation of potassium chloride to potassium sulphate with the release of a high partial pressure of chlorine can take place both at the oxide-deposit interface and near the deposit surface.[40] Most of the released chlorine will diffuse into the atmosphere, whereas a fraction diffuses inward resulting in corrosion.[2] However the presence of KCl in an oxidising environments (O_2+H_2O+O_2) without SO_2 can result in similar corrosion attack, as KCl can also react directly with oxides to release corrosive Cl species.[15,41]

3.4.2. Temperature data comparison

The temperature data during the exposure period from Randers and MSK (Figures 2-5) show significant differences. The average test tube steam outlet temperature in Randers was 512 ^{o}C, while in MSK it was 544 ^{o}C. The significantly higher average steam temperature at MSK than at Randers would obviously increase the degree of fireside corrosion. Randers also has a broader temperature range with a significant amount of hours below 500ºC where there would be minimal corrosion for an austenitic steel. As has been previously observed for these types of steels,[5] corrosion increases significantly with increase in temperature and this is probably the main reason for the higher corrosion rates of the steel tubes observed for the MSK plant (Table 4). Another important factor is the thermal cycling of the plants. The plant in Randers has only had one shutdown during the entire exposure period and otherwise the operation temperature has been relative stable (Figure 2). This is in complete contrast to the MSK plant where frequent thermal cycling resulted in severe exposure conditions. At the MSK plant there has been three full shutdowns, but during autumn and late spring, there was thermal cycling every day between 200 and 540 ^{o}C (Figure 3 and Figure 4) resulting in 213 start/stop cycles (Table 2). This is with high certainty the reason behind the spallation of both Ni and Ni_2Al_3 coatings in the MSK boiler.

The present work shows that the performance of the coatings is related to the specific operation conditions of the different plants. For the MSK plant, the frequent temperature cycling is a huge challenge for any coating. A very close fit in thermal expansion coefficients between steel and coating would be necessary for any coating to survive in this condition. For the Randers plant, this is of less importance since almost no cycling is carried out, which implies that this type of plant is a more obvious candidate for life time extension through coating application. In fact, application of a simple electroplated Ni-coating helped lower the metal loss from 23 μm to 3.37 μm in the Randers plant. This could indicate that biomass fired power plants with certain characteristics (low amount of temperature cycling, intermediate average temperature and fuel with intermediate corrosiveness) could benefit from application of simple Ni-coatings, whereas the application of coating systems to the most aggressively run plants remains a huge challenge.

4. Conclusions

1. The reference uncoated tubes were more heavily attacked at MSK plant than at Randers plant. For the exposure in MSK, the average metal loss and corrosion rate were almost 30 times higher than in Randers.

2. The Ni and Ni_2Al_3 coatings showed better corrosion resistance than uncoated steel in Randers. The Ni_2Al_3 coatings were still present in most areas with only localized attack.

3. The corrosion performance of Ni and Ni_2Al_3 coatings was not satisfactory for the exposure conditions at the MSK plant. The Ni_2Al_3 coatings spalled off and were only found as remnants in the deposit. The spallation was with high certainty linked to the frequent thermal cycling in the MSK plant.

4. The combination of higher outlet steam temperature, more corrosive fuel and more severe thermal cycling results in unsatisfactory coating performance in MSK. However, for the less aggressive conditions in Randers the application of a simple Ni-coating had beneficial effects.

Acknowledgements

References

(1) Antunes, R. A.; de Oliveira, M. C. L. Corrosion in Biomass Combustion: A Materials Selection Analysis and Its Interaction with Corrosion Mechanisms and Mitigation Strategies. *Corros. Sci.* **2013**, *76*, 6–26.

(2) Nielsen, H. P.; Frandsen, F. J.; Dam-Johansen, K.; Baxter, L. L. Implications of Chlorine-Associated Corrosion on the Operation of Biomass-Fired Boilers. *Prog. Energy Combust. Sci.* **2000**, *26* (3), 283–298.

(3) Grabke, H. J.; Zahs, A.; Spiegel, M. The Influence of Alloying Elements on the Chlorine-Induced High Temperature Corrosion of Fe-Cr Alloys in Oxidizing Atmospheres. *Mater. Corros.* **1999**, *50* (10), 561–578.

(4) Zahs, A.; Spiegel, M.; Grabke, H. J. Chloridation and Oxidation of Iron, Chromium, Nickel and Their Alloys in Chloridizing and Oxidizing Atmospheres at 400-700°C. *Corros. Sci.* **2000**, *42* (6), 1093–1122.

(5) Montgomery, M.; Karlsson, A.; Larsen, O. H. Field Test Corrosion Experiments in Denmark with Biomass Fuels Part I: Straw-Firing. *Mater. Corros.* **2002**, *53* (2), 121–131.

(6) Stott, F. H.; Shih, C. Y. High-Temperature Corrosion of Iron-Chromium Alloys in Oxidizing-Chloridizing Conditions. *Oxid. Met.* **2000**, *54* (5–6), 425–443.

(7) Li, Y. S.; Sanchez-Pasten, M.; Spiegel, M. High Temperature Interaction of Pure Cr with KCl. *Mater. Sci. Forum* **2004**, *461–464*, 1047–1054.

(8) Pan, T. J.; Zeng, C. L.; Niu, Y. Corrosion of Three Commercial Steels under ZnCl2-KCl Deposits in a Reducing Atmosphere Containing HCl and H$_2$S at 400-500°C. *Oxid. Met.* **2007**, *67* (1–2), 107–127.

(9) Andersson, P.; Norell, M. Scale Growth on Austenitic Alloys under KCl Deposits at 500°C. *Mater. Sci. Forum* **2008**, *595–598*, 333–342.

(10) Lu, W. M.; Pan, T. J.; Zhang, K.; Niu, Y. Accelerated Corrosion of Five Commercial Steels under aZnCl2–KCl Deposit in a Reducing Environment Typical of Waste Gasification at 673-773 K. *Corros. Sci.* **2008**, *50* (7), 1900–1906.

(11) Pettersson, J.; Svensson, J. E.; Johansson, L. G. Alkali Induced Corrosion of 304-Type

Austenitic Stainless Steel at 600 Degrees C; Comparison between KCl, K_2CO_3 and K_2SO_4. *Mater. Sci. Forum* **2008**, *595–598*, 367–375.

(12)   Lee, Y. Y.; McNALLAN, M. J. Ignition of Nickel in Environments Containing Oxygen and Chlorine. *Metall. Trans. A* **1987**, *18A* (6), 1099–1107.

(13)   Grabke, H. J.; Reese, E.; Spiegel, M. The Effects of Chlorides, Hydrogen Chloride, and Sulfur Dioxide in the Oxidation of Steels below Deposits. *Corros. Sci.* **1995**, *37* (7), 1023–1043.

(14)   Pettersson, J.; Asteman, H.; Svensson, J. E.; Johansson, L. G. KCl Induced Corrosion of a 304-Type Austenitic Stainless Steel at 600 °C; the Role of Potassium. *Oxid. Met.* **2005**, *64* (1–2), 23–41.

(15)   Pettersson, J.; Svensson, J. E.; Johansson, L. G. KCl-Induced Corrosion of a 304-Type Austenitic Stainless Steel in O_2 and in O_2 + H_2O Environment: The Influence of Temperature. *Oxid. Met.* **2009**, *72* (3–4), 159–177.

(16)   Saeed; Kiamehr. Material Solutions to Mitigate the Alkali Chloride-Induced High Temperature Corrosion, PhD thesis, Technical University of Denmark, 2014.

(17)   Li, Y. S.; Spiegel, M. Internal Oxidation of Fe–Al Alloys in a KCl-Air Atmosphere at 650°C. *Oxid. Met.* **2004**, *61* (3–4), 303–322.

(18)   Li, Y. S.; Spiegel, M.; Shimada, S. Corrosion Behaviour of Various Model Alloys with NaCl-KCl Coating. *Mater. Chem. Phys.* **2005**, *93* (1), 217–223.

(19)   Kiamehr, S.; Lomholt, T. N.; Dahl, K. V.; Christiansen, T. L.; Somers, M. A. J. Application of Aluminum Diffusion Coatings to Mitigate the KCl-Induced High-Temperature Corrosion. *Mater. Corros.* **2016**, No. 1, 82–94.

(20)   Dahl, K. V.; Slomian, A.; Lomholt, T. N.; Kiamehr, S.; Grumsen, F. B.; Jonsson, T. Characterization of Pack Cemented Ni_2Al_3 Coating Exposed to KCl (S) Induced Corrosion at 600 ° C. *Mater. High Temp.* **2017**, *3409* (October), 1–8.

(21)   Vokál, V.; Rohr, V.; Pomeroy, M. J.; Schütze, M. Corrosion of Alloys and Their Diffusion Aluminide Coatings by KCl:K_2SO_4 Deposits at 650°C in Air. *Mater. Corros.* **2008**, *59* (5), 374–379.

(22) Jonsson, T.; Slomian, A.; Lomholt, T. N.; Kiamehr, S.; Dahl, K. V. Microstructural Investigations of Pure Nickel Exposed to KCl Induced High Temperature Corrosion. *Mater. High Temp.* **2015**, *32* (1–2), 44–49.

(23) https://www.materials.sandvik/en/materials-center/material-datasheets/.

(24) Petersen, S. S. CFD Modelling of a Biomass Incinerator for Prediction of Risk Areas for Corrosion Damages, Technical University of Denmark, 2012.

(25) https://www.ecn.nl/phyllis2/Browse/Standard/ECN-Phyllis.

(26) Henriksen, N.; Vilhelmsen, T.; Larsen, O. H.; Blum, R. Oxide Growth and Temperature Increase in Evaporators of Supercritical PF Boilers. *VGB PowerTech* **1999**, *79*, 71–77.

(27) Delaey, L.; Tas, H. Hot Isostatic Pressing 93; Elsevier Science B.V: Amsterdam, 1994; pp 301–308.

(28) Wu, D. L.; Dahl, K. V; Christiansen, T. L.; Montgomery, M.; Hald, J. Microstructural Investigations of Ni and Ni_2Al_3 Coatings Exposed in Biomass Power Plants. *Mater. High Temp.* **2017**.

(29) Okoro, S. C. High Temperature Corrosion on Biodust Firing, PhD thesis, Technical University of Denmark, 2016.

(30) Broström, M.; Enestam, S.; Backman, R.; Mäkelä, K. Condensation in the KCl-NaCl System. *Fuel Process. Technol.* **2013**, *105*, 142–148.

(31) Lindberg, D.; Niemi, J.; Engblom, M.; Yrjas, P.; Laurén, T.; Hupa, M. Effect of Temperature Gradient on Composition and Morphology of Synthetic Chlorine-Containing Biomass Boiler Deposits. *Fuel Process. Technol.* **2016**, *141*, 285–298.

(32) Jensen, P. A.; Frandsen, F. J.; Dam-Johansen, K.; Sander, B. Experimental Investigation of the Transformation and Release to Gas Phase of Potassium and Chlorine during Straw Pyrolysis. *Energy & Fuels* **2000**, *14* (7), 1280–1285.

(33) Larsen, O. H.; Jensen, J. P.; Biede, O.; Montgomery, M.; Andersson, C. Relations between Combustion, Deposition, Flue Gas Temperatures and Corrosion in Straw-Fired Boilers. In *2nd World Conference and Technology Exhibition on Biomass for Energy and Industry*; Rome, 2004; p OD7.2.

(34)   Zhou, H.; Jensen, P. A.; Frandsen, F. J. Dynamic Mechanistic Model of Superheater Deposit Growth and Shedding in a Biomass Fired Grate Boiler. *Fuel* **2007**, *86* (10–11), 1519–1533.

(35)   Pettersson, J.; Folkeson, N.; Johansson, L. G.; Svensson, J. E. The Effects of KCl, K$_2$SO$_4$ and K$_2$CO$_3$ on the High Temperature Corrosion of a 304-Type Austenitic Stainless Steel. *Oxid. Met.* **2011**, *76* (1–2), 93–109.

(36)   Wen, Z.; Zhao, Y.; Hou, H.; Tian, J.; Han, P. First-Principles Study of Ni-Al Intermetallic Compounds under Various Temperature and Pressure. *Superlattices Microstruct.* **2017**, *103*, 9–18.

(37)   Karunaratne, M. S. A.; Kyaw, S.; Jones, A.; Morrell, R.; Thomson, R. C. Modelling the Coefficient of Thermal Expansion in Ni-Based Superalloys and Bond Coatings. *J. Mater. Sci.* **2016**, *51* (9), 1–14.

(38)   Krause, H. H. High Temperature Corrosion in Waste Incineration Systems. *J. Mater. Energy Syst.* **1985**, *7* (4), 322–332.

(39)   Salmenoja, K.; Makela, K. Prevention of Superheater Corrosion in the Combustion of Biofuels. *Corrosion* **2000**, No. 149, No.238.

(40)   Okoro, S. C.; Montgomery, M.; Frandsen, F. J.; Pantleon, K. Effect of Water Vapor on High-Temperature Corrosion under Conditions Mimicking Biomass Firing. *Energy and Fuels* **2015**, *29* (9), 5802–5815.

(41)   Okoro, S. C.; Kiamehr, S.; Montgomery, M.; Frandsen, F. J.; Pantleon, K. Effect of Flue Gas Composition on Deposit Induced High Temperature Corrosion under Laboratory Conditions Mimicking Biomass Firing. Part II: Exposures in SO$_2$ Containing Atmospheres. *Mater. Corros.* **2017**, *68* (5), 515–528.

Abstract Graphics:

Straw firing power plant
Thermal cycling + 540 ^{o}C

Wood firing power plant
No Thermal cycling + 520 ^{o}C
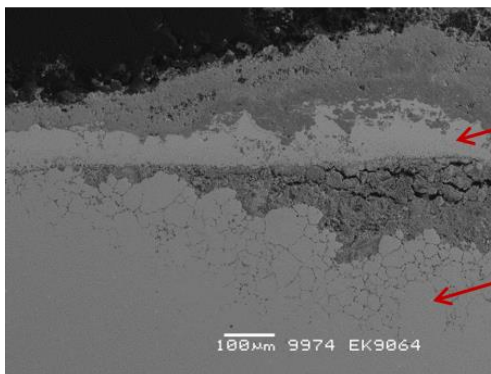
Ni$_2$Al$_3$ coating

Ni coating

steel

100 µm